

Electron wave-function spillover in self-assembled InAs/InP quantum wires

J. Maes* and M. Hayne

Pulsed Field Group, Laboratory of Solid State Physics and Magnetism, K.U. Leuven, Celestijnenlaan 200D, B-3001 Leuven, Belgium

Y. Sidor, B. Partoens, and F. M. Peeters

Departement Natuurkunde, Universiteit Antwerpen (Campus Drie Eiken), Universiteitsplein 1, B-2610 Antwerpen, Belgium

Y. González, L. González, D. Fuster, and J. M. García

Instituto de Microelectrónica de Madrid (CNM-CSIC), C/Isaac Newton 8, 28760 Tres Cantos, Madrid, Spain

V. V. Moshchalkov

Pulsed Field Group, Laboratory of Solid State Physics and Magnetism, K.U. Leuven, Celestijnenlaan 200D, B-3001 Leuven, Belgium

(Received 4 December 2003; revised manuscript received 19 February 2004; published 15 October 2004)

Charge confinement in InAs/InP self-assembled quantum wires is studied experimentally using photoluminescence in pulsed magnetic fields and theoretically using adiabatic theory within the effective-mass approximation, taking into account the strain in the samples. We show both experimentally and theoretically that, in spite of the large conduction band offset, the electron wave function is significantly spilled out of the wire in the wire height direction for thin wires. Furthermore, for a wire thickness of up to 8 monolayers, the electron spillover is inversely related to the wire height. These effects are due to the large zero point energy of the electron. As the wire becomes thicker, the decrease in confinement energy is reflected in a reduction of the electron wave-function extent.

DOI: 10.1103/PhysRevB.70.155311

PACS number(s): 73.21.La, 78.55.Cr, 78.67.Hc

I. INTRODUCTION

Under certain growth conditions, uniform arrays of self-assembled quantum wires can be obtained by solid source molecular beam epitaxial (MBE) deposition of InAs on an InP substrate.¹⁻⁴ InAs quantum wires embedded in an InP matrix are a type-I system, and act to confine the electron and hole to the InAs wires.⁵ They are promising candidates for optical applications at the telecommunication wavelengths (1.3 and 1.55 μm), although they generally show a broad photoluminescence (PL) spectrum consisting of several peaks that are attributed to quantum wires of heights which differ by a discrete number of monolayers.² Here, information on the confinement of excitons in such wires is obtained by careful analysis of the energy shift of the PL peaks in high magnetic fields (≤ 50 T) and by a strain dependent effective-mass approximation.⁶⁻⁸ Although both conduction and valence band offsets are large (0.657 and 0.35 eV, respectively) and thus electrons and holes are expected to be strongly confined to the InAs wire, we find that for very flat wires a large fraction of the electron wave function is located in the InP barrier material. In this regime, the exciton wave-function extent is inversely related to the wire height. Such a wave-function penetration into the barrier material has already been predicted and observed for $\text{In}_{0.1}\text{Ga}_{0.9}\text{As}/\text{GaAs}$ quantum wells,⁹ T- and V-shaped GaAs quantum wires,¹⁰⁻¹³ Ge/Si quantum dots,¹⁴ and other nanostructures, where the charge confinement is relatively weak in the absence of a magnetic field:^{15,16} much weaker than in the InAs/InP quantum wires under study. In these systems, the wave-function spillover was investigated mainly

theoretically^{10,12,16} or by PL in zero field¹⁴ or low magnetic fields up to 12 T.^{9,11} A detailed overview of exciton confinement in GaAs quantum wires is given by Akiyama.¹³ In addition, the dependence of the wave-function penetration on the dimensionality of the system was studied and shows that, due to the lower dimensionality of the quantum wire, the confinement energy is increased and thus the wave-function penetration into the barrier is larger as compared to a quantum well with similar band offsets.^{10,15,17} Three methods of fabricating quantum wires, other than the self-assembly process mentioned here, have been applied to the In(Ga)As/InP system. The first is the deposition of an unstrained $\text{In}_{0.53}\text{Ga}_{0.47}\text{As}/\text{InP}$ multi-quantum-well on a vicinal (001) InP substrate, which leads to very thin quasi-one-dimensional filaments¹⁸ in which exciton wave function penetration is expected due to the monolayer thickness,⁸ but to date, has not been quantitatively studied. A second method is based on the deposition of a lithographically patterned stressor on top of an InGaAs/InP quantum well,¹⁹ and the third method relied on the pre patterning of the substrate.²⁰ In this way, large quantum wires have been created for which, consequently, no wave-function penetration is expected. In the self-assembled InAs/InP system (both wires and dots), a wave-function spillover into the barrier material was not expected and thus had not been considered to date,^{2,21,22} but it has important consequences for applications. To improve the performance of lasers based on InAs/InP wire structures, the growth procedure should be adjusted to allow higher wires to develop uniformly in which there is a reduced wave-function spillover, an enhanced electron-hole overlap and an improved carrier confinement.

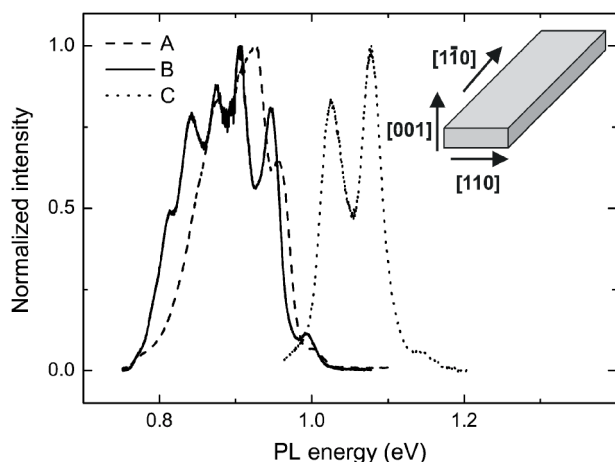


FIG. 1. Zero-field spectra for the samples A (dashed), B (solid), and C (dotted). The inset shows a schematic representation of the wire with the different crystallographic directions.

II. GROWTH OF QUANTUM WIRES

We report on the investigation of three different quantum wire samples. The first sample (A) was fabricated by atomic layer molecular beam epitaxy. A 200 nm thick InP buffer layer was grown on top of an InP substrate at 430 °C. The temperature was kept constant during the deposition of 2.5 monolayers (ML) of InAs. The sample was subsequently annealed for 2 min at 530 °C. For this sample, it was during the annealing that the quantum wires formed. Afterwards, the temperature was lowered again to the original value for deposition of the 50 nm thick InP capping layer. For the second sample (B), the growth was similar but at different temperatures. The deposition temperature was 430 °C and the annealing temperature was 560 °C. In sample C, InAs was grown at 515 °C. In this sample, due to the elevated temperature, quantum wires were formed during growth after 1.7 ML of InAs was deposited, without any further annealing step. Immediately after wire formation, the InAs growth was interrupted and a 20 nm InP cap layer was grown at the same temperature. In all samples, the InAs quantum wires are oriented along the $[1\bar{1}0]$ direction with a height that is an order of magnitude thinner than the width^{1,2} (Fig. 1, inset).

The basis of the formation of quantum wires rather than dots is an anisotropy in the built-in stress at the InAs/InP(001) interface,¹ where the stress is higher in the $[110]$ direction than along $[1\bar{1}0]$. In this way, when an InAs monolayer is grown, the distorted In-As bonds contribute to the appearance of a compressive stress in the $[110]$ direction, while no stress appears in the $[1\bar{1}0]$ direction. Further deposition of InAs increases the compressive stress equally in both directions, and as a result, the critical amount of stress necessary to cause relaxation is first reached in the $[110]$ direction. Therefore, wires form that are oriented in the $[1\bar{1}0]$ direction. The relaxation of the epitaxial stress in the $[110]$ direction amounts to $\sim 20\%$ of the total accumulated stress during growth [1]. Quantum wire formation is characteristic of solid-source MBE growth under group V stabilized (2×4 reconstruction) surface for heteroepitaxial systems with

different group V elements. Growing under other surface conditions or other growth procedures (metalorganic chemical vapor deposition, chemical beam epitaxy, and gas-source MBE) results in the usual quantum dot formation.

An estimate of the size and shape of the wire can be made by analyzing atomic force microscopy (AFM) images on similar but uncapped structures. These show a wire period of 24 nm, a wire width of 18 nm, and an average vertical peak-to-valley amplitude of 1.4 nm.^{1,2} The typical length exceeds 1 μm . Since the height is much smaller than the width, the wires can be regarded as ribbons. While the width is more or less constant, the height varies substantially between 0.6 and 2.0 nm for different wires. Therefore, a broad luminescence spectrum is expected, and the different PL peaks in samples B and C (Fig. 1) can be attributed to wires of different heights of a discrete number of monolayers.² Such a monolayer splitting was also recently observed in InAs/GaAs (Ref. 23) and InAs/InP quantum dots.²¹ It is found that the geometric characteristics of the uncapped wires are independent of variations in growth conditions such as those of the three samples studied. Due to the capping process, however, a temperature dependent As/P exchange occurs at the surface.⁴ In sample C, which has the highest growth temperature of the InP cap layer, this exchange process is most pronounced, reducing the amount of InAs incorporated in the wires. Therefore, the smallest wires are expected for sample C, and from its large zero-field PL energy, a smaller wire height is indeed inferred. The fact that only two pronounced peaks are present reflects a reduced distribution in the wire height.

III. EXPERIMENTAL AND THEORETICAL METHOD

The photoluminescence experiments were carried out at 4.2 K in a helium bath cryostat that is placed in the bore of a pulsed magnet. Excitation light, provided by a Nd:yttrium aluminum garnet laser operating at 532 nm, was focused into a 200 μm core optical fiber. At the cryostat end, six detection fibers placed around the excitation fiber collected the luminescence from the sample, which was then dispersed in a 0.3 m spectrometer coupled to an InGaAs diode array detector. The magnetic field B can be applied parallel to the growth direction ($B//[011]$), parallel to the wires ($B//[1\bar{1}0]$) or perpendicular to both ($B//[110]$, see the inset of Fig. 1). In the latter two cases, the sample is mounted vertically and a mirror is placed at 45° to increase the luminescence intensity that is picked up by the fibers. In a ~ 20 ms field pulse, up to 4 spectra were taken at different values of the field, each with a 0.5 ms photon integration time and a field variation that is $\pm 3\%$ at most.

Applying a magnetic field provides information on the exciton confinement in the plane perpendicular to B . The InAs/InP quantum wires are clearly not cylindrically symmetric in this plane for any direction of the field. In such a case, the diamagnetic energy shift is determined mainly by the direction of strongest confinement in the plane perpendicular to B .²⁴ For example, with B along $[001]$ the confinement in the direction of the width is probed (Fig. 1, inset).

And if B is applied along the width, i.e., along [110], information about the wire height can be gained. If one of the charge carriers of the exciton (either electron or hole) has a very different extent than the other, the diamagnetic shift will, in general, be determined by the particle with the largest extent.

The diamagnetic energy shift generally has a parabolic field dependence at low magnetic fields that is given by $\Delta E = e^2 \langle \rho^2 \rangle B^2 / 8\mu$, where $\langle \rho^2 \rangle^{1/2}$ and μ are the exciton radius and effective mass, respectively, in the plane perpendicular to the field. For a noncylindrically symmetric system, $\langle \rho^2 \rangle^{1/2}$ should be regarded as an averaged radius in the direction of the strongest confinement only, as mentioned above. For sufficiently high fields, when the magnetic length becomes smaller than the spatial confinement, the magnetic confinement will dominate and a linear behavior is observed parallel to the lowest Landau level: $\Delta E \propto \hbar e B / 2\mu$. Combining these formulas into a single function, with the requirement that this function and its derivative is continuous, generates a unique set of values for $\langle \rho^2 \rangle^{1/2}$ and μ .²⁵ With l_c the magnetic length [$l_c = (\hbar / eB)^{1/2}$] at the crossover field between the two regimes, the exciton radius can be written as $\langle \rho^2 \rangle^{1/2} = \sqrt{2}l_c$. Other methods that combine the low and high field limit more gradually, such as that presented by Janssens *et al.*²⁶ and a description via Fock-Darwin states²⁷ are found to produce similar $\langle \rho^2 \rangle^{1/2}$ and μ . However, when the high field limit is not entirely reached, all three models fail, even when a deviation from the parabolic field dependence is already clearly observed; i.e., when the ΔE is plotted as a function of B^2 . Due to the small heights of the InAs/InP quantum wires, the crossover between parabolic and linear field dependence occurs at high magnetic field when B is perpendicular to [001]. This results in only a small deviation from parabolic behavior in the 0–50 T range. Therefore, in this work, the aforementioned set of expressions from Ref. 25 are used only to detect the *onset* of this “crossover field” regime rather than to quantify the exciton radius and mass. We find that, compared to the two other models, this model is the most sensitive to the deviation from parabolic behavior, and

TABLE I. Material parameters for InAs and InP used in the calculations.

Parameters	InAs	InP
Lattice constant (Å)	6.058	5.869
Bandgap (eV)	0.417	1.424
Electron mass (m_0)	0.026	0.08
Hh mass along [110] (m_0)	0.513	0.885
Hh mass along [001] (m_0)	0.333	0.532
a_c (eV)	-5.08	...
a_v (eV)	1	...
b (eV)	-1.8	...
d (eV)	-3.6	...
Strain coefficient C_{11} (GPa)	83.29	...
Strain coefficient C_{12} (GPa)	45.26	...
Dielectric constant	15.15	12.5

gives a crossover field that corresponds well with that seen in plots of ΔE versus B^2 . Since the crossover field regime is inversely proportional to the exciton radius and independent of the exciton effective mass, the field at which this deviation is detected directly provides qualitative information on the exciton extent. Quantitatively, however, the uncertainty is due to the small size of the deviation from the parabolic field behavior and would be improved if higher magnetic fields could be applied.

In our calculations, we used the adiabatic approximation within the effective-mass theory to calculate the exciton energy of an electron-hole pair in a rectangular quantum wire. The conduction and valence band offsets are taken to be $E_c = 0.657$ eV and $E_v = 0.35$ eV.⁵ To include the strain, which shifts the electron and hole confinement potentials, we used the expressions for the strain tensor of Ref. 6. The edge of the conduction band is shifted by the hydrostatic strain

$$E_c = E_{c0} + a_c \varepsilon_{hyd},$$

where a_c denotes the hydrostatic deformation potential for the conduction band. The heavy hole (hh) and light hole (lh) band edges are calculated from the Pikus-Bir Hamiltonian⁷

$$E_{vhh} = E_v + P + \text{sgn}(Q) \sqrt{Q^2 + RR^* + SS^*},$$

$$E_{vhl} = E_v + P - \text{sgn}(Q) \sqrt{Q^2 + RR^* + SS^*},$$

where P , Q , R , and S are matrices that depend on the deformation potentials a_v , b , and d of the valence band. We found that the heavy hole will be the hole ground state due to the shear separation potential, as in the case of a quantum well. We approximated the heavy hole confinement potential by a rectangular shape in which the depth was determined by its value in the center of the wire. This simplifies our calculation and we checked that including the nonrectangular shape only changes the hole energy by less than 2%.

Different anisotropic effective masses are assumed inside and outside of the InAs/InP quantum wire and along the [001] and the [110] directions. In the adiabatic approach, one first solves the one-dimensional problem in the narrow [001] direction, and then uses the energy level found as the bottom of the potential well for a second one-dimensional problem in the other [110] direction.⁸ This approach yields very good results as long as there is an appreciable difference in confinement widths,⁸ which is certainly the case for the wires studied here. The Coulomb interaction between the electron and the hole is not included as it is a small correction: from the formula for the upper bound of the exciton binding energy in a quantum well, this correction is estimated to be less than 9 meV.²⁸ All physical parameters used are listed in Table I and are taken from Refs. 5 and 29.

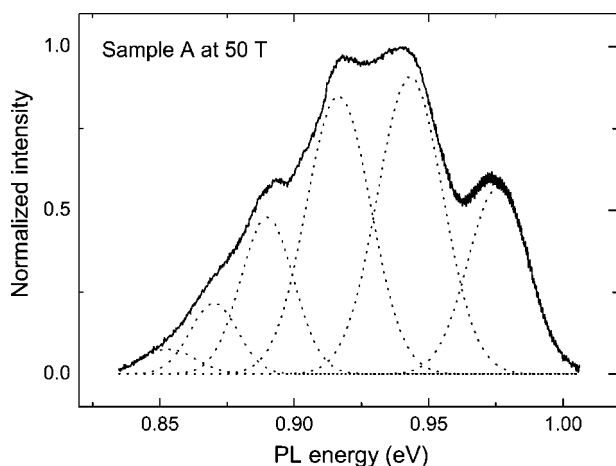


FIG. 2. In a high field of 50 T, the different contributions to the PL of sample A become narrower and are clearly distinguishable. The dotted lines are the fitted Gaussian contributions.

IV. EXPERIMENTAL VERSUS NUMERICAL RESULTS AND DISCUSSION

Recombination of electrons and holes in the wires results in photoluminescence with photon energies ranging from 0.7–1.2 eV for the three samples (Fig. 1). The samples A and B, grown at low temperature, have a broad PL signal, in which, for sample A, a clear distinction between the different contributions cannot be made. For sample B there are at least six Gaussian peaks present. Sample C has only two pronounced peaks at higher energies. It is apparent from the number of peaks that the growth conditions for sample C improve the homogeneity in wire height.

At zero field, sample A reveals a broad spectrum (122 meV overall width) with hardly any visible structure (Fig. 1). If a magnetic field of 50 T is applied parallel to the growth direction [001], the various contributions to the PL become distinguishable (Fig. 2). Since the overall width decreases to 95 meV, the peaks are not separated by the field, meaning that the individual PL peaks become discernable because they narrow in field. Since this effect is insignificant when the field is applied in the growth plane, it shows that for sample A, the zero-field linewidth of the different contributions is determined mostly by variations of the wavefunction extent in the growth plane; i.e., by the inhomogeneity in the width of the wires.

The different contributions to the PL from sample B can already be seen at zero field. This shows that the size inhomogeneity in the growth plane has improved substantially compared to that of sample A. It is therefore possible to compare the experimental peak energies with those expected from numerical calculations, using the assumption that the PL peaks originate from wires of different heights that vary by a discrete number of monolayers.² Taking into account that the exciton ground state is expected to consist of an electron bound to a heavy hole, the best correspondence in peak separation is found for wire heights from 6 to 13 ML (1 ML=0.303 nm for bulk InAs) for the high- to low-energy peaks, respectively, and with the calculated peak energies shifted up by 39 meV (Fig. 3). Such a shift is justified be-

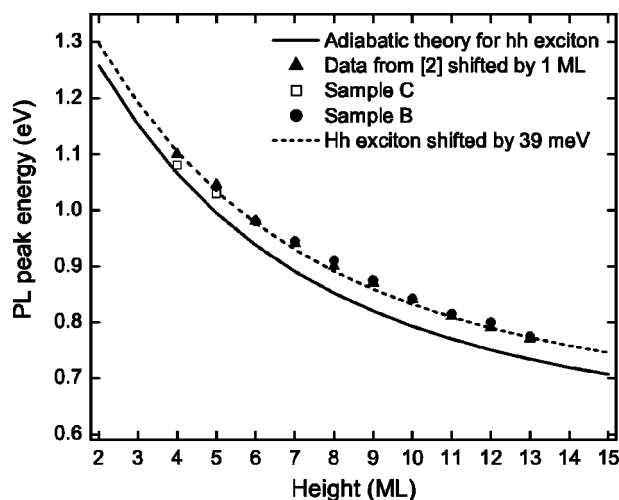


FIG. 3. PL peak energies as a function of the quantum wire height in the adiabatic approximation for heavy hole excitons (solid). The circles correspond to the peak positions for sample B and the squares to those of sample C. The triangles represent data from Ref. 2 and are shifted to the left by one monolayer. The dashed curve shows the calculated heavy-hole exciton PL peak energies shifted up by 39 meV.

cause of the uncertainty in the band offsets.⁵ In comparison with data obtained on other samples and with values calculated using an eigenfunction expansion method (as reported in Ref. 2), we find that the peaks originate from wires that are one monolayer thinner, which is in better correspondence with the heights obtained by AFM for those data.²

The overall broadness of sample B complicates the analysis of the in-field data due to technical limitations. Therefore, qualitative results are only obtained for the peak at 0.94 eV, which is the most intense and has a relatively large separation from the other peaks. From Fig. 3, the PL at 0.94 eV is

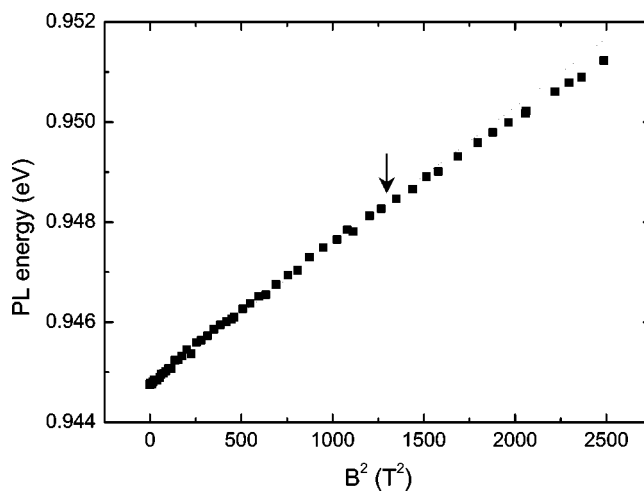


FIG. 4. PL peak energy as function of the square of the magnetic field ($B/[110]$) for the 0.94 eV peak of sample B. The solid line is the extrapolation of a linear fit between 0 and 1300 T². The deviation of the data from the straight line, indicated by the arrow, demonstrate a nonparabolic field dependence of the ΔE and thus a relatively large exciton radius.

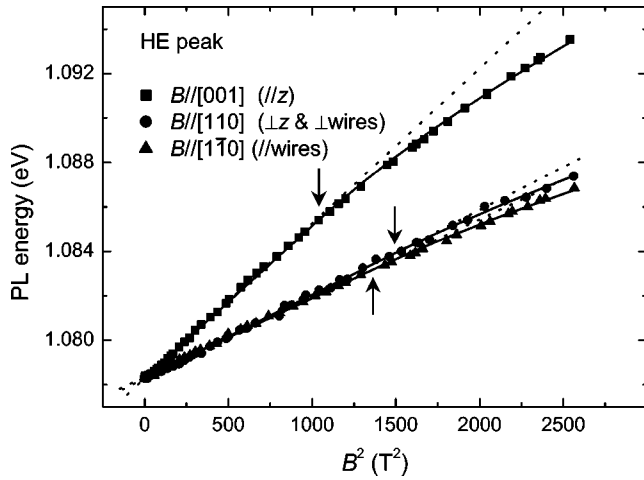


FIG. 5. The same as Fig. 4, but now for the HE peak of sample C where the magnetic field is applied along the three different crystallographic directions indicated in the inset of Fig. 1. The arrows indicate the crossover fields. The dashed lines are extrapolations of the parabolic field dependence.

assigned to annihilation of an exciton bound to a 7 ML (or 2.1 nm) high wire. When applying a magnetic field parallel to [110], the exciton wave-function extent in the direction of the wire height is investigated, and thus a parabolic field dependence of the diamagnetic shift might be expected up to 50 T due to the small wire height. However, when the PL energy is plotted against B^2 (Fig. 4) a clear deviation from the linear behavior is detected. The exciton wave-function size is thus much larger than the wire height of 2.1 nm. A magnetic length of 2.1 nm corresponds to 149 T, whereas the deviation starts at 36 T, as indicated by the arrow in Fig. 4. Such a field gives a magnetic length of 4.3 nm and a $\langle \rho^2 \rangle^{1/2}$ of 6.0 nm using the model from Ref. 25. The data therefore demonstrate that the quantum wire is too thin to enclose a large portion of the wave function, which must be partially located in the InP matrix above and/or below the InAs wire. Such a penetration of the wave function into the barrier material is common in nanostructures that have weak charge localization, such as in GaAs/AlGaAs quantum wires formed by junction of quantum wells¹⁰ or by a bend in a well,^{11,12} but was not anticipated in the samples under study due to the large conduction and valence band offsets of 657

TABLE II. PL energies, crossover fields, and associated exciton extents for the two pronounced peaks of sample C and all three field directions.

Peak	Field direction	Crossover field (T)	Exciton extent (nm)
LE (1.03 eV)	[001] ($B//z$)	37.7	5.9
	[110] ($B//wires$)	43.5	5.5
	[110]	≥ 43.5	≤ 5.5
HE (1.08 eV)	[001] ($B//z$)	32.1	6.4
	[110] ($B//wires$)	36.7	6.0
	[110]	38.6	5.8

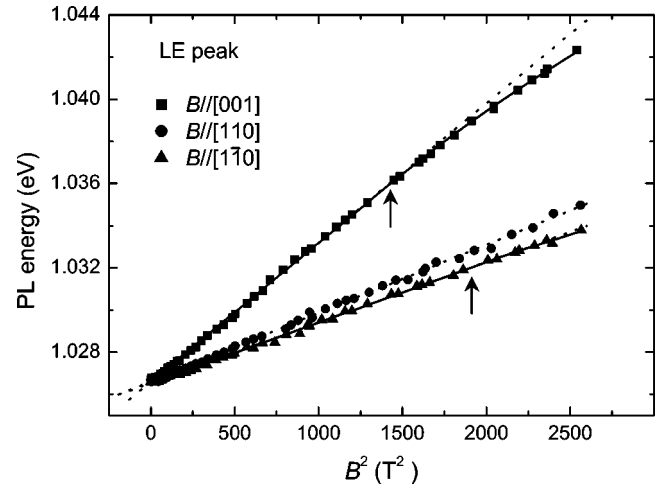


FIG. 6. The same as Fig. 5, but now for the LE peak of sample C.

and 350 meV, respectively. For comparison, the conduction band offset is 225 meV for GaAs/Al_{0.3}Ga_{0.7}As quantum wires,¹² 79 meV for In_{0.1}Ga_{0.9}As/GaAs quantum wells,⁵ and 120 meV for Ge/Si quantum dots.¹⁴

Sample C, which has a less broad overall spectrum and well-separated peaks, is best suited for analysis of the diamagnetic energy shift. Due to the low number of peaks, it is not possible to compare the curvature in peak energy versus wire height with the numerical PL energies of Fig. 3. However, because of the larger growth temperature, and thus a larger As/P exchange during the capping procedure,⁴ there is less InAs present in the wire than for sample B, and reduced dimensions are expected for the wire height and/or width. By comparing the PL energies with those of sample B, wire heights of 4 and 5 ML are estimated for the high-energy (HE) and low-energy (LE) peaks, respectively (Fig. 3). In Fig. 5 the PL energy of the HE peak is plotted as a function of B^2 for all three field directions. They are analyzed with aforementioned set of expressions²⁵ and the dashed lines are the extrapolation of the parabolic dependence. It is clear from these extrapolations that all three curves deviate from a linear B^2 dependence. The crossover fields as provided by our model are given in Table II, together with the corresponding exciton extents. Note that, as mentioned in Sec. III, for crossover fields this close to the maximum obtainable field, these sizes are a qualitative measure of the exciton extent rather than of the real exciton radius. For $B//[110]$, the clear deviation from the linear B^2 behavior for the HE peak reflects the vertical spread of the wave function into the InP, which we also observed for sample B. Since in the (110)

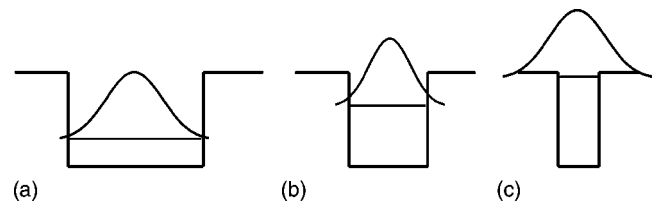


FIG. 7. Schematic drawing of the change in confinement with wire height.

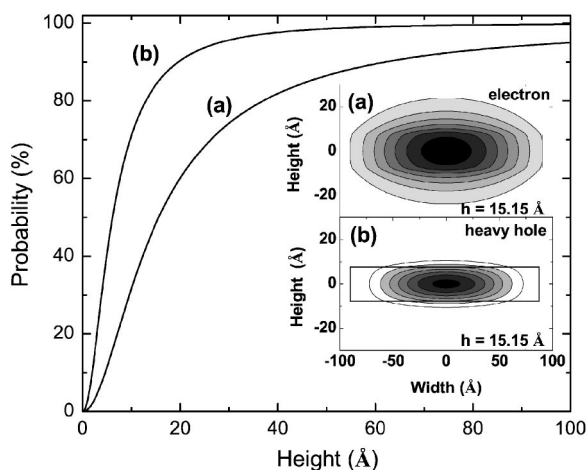


FIG. 8. Probability of (a) the electrons and (b) the heavy holes to be inside the quantum wire as a function of the wire height. The insets are the contour plots of the (a) electron and (b) heavy-hole wave functions confined to a quantum wire with height 5 ML (15.15 Å) and width 180 Å.

plane (the wire cross section), the direction of strongest confinement is [001], the diamagnetic shift with a field applied along [110] resembles most that of the B//[110] situation, as can be seen in Fig. 5 and Table II.

The LE peak of sample C has a less obvious sublinear dependence on B^2 for B//[110], and for B//[110] a deviation from the linear behavior is not even detected (Fig. 6). The latter means that the crossover field is larger than that for B//[110] and thus that 5.5 nm is an upper limit for the exciton extent in the wire height direction (Table II). If we now compare the exciton extents for B//[110] and both peaks, we observe a decrease from 5.8 to ≤ 5.5 nm for increasing wire height. This means that the exciton extent significantly decreases as the wires become thicker and a larger portion of the exciton wave function is confined to the InAs quantum wire.

The inverse relation of the exciton extent to the wire height is clarified by Fig. 7, where a schematic diagram of a wave function confined to a nanostructure is given. If the potential well is not too narrow, a decrease in size leads to a shrinkage of the wave-function extent; i.e., in Fig. 7(b) the extent is smaller than in Fig. 7(a). However, if it is made even thinner, the confinement energy becomes comparable to the band offset. This causes the wave function to significantly spread out into the barrier material and thus to increase its extent with decreasing wire height [compare Figs. 7(b) and 7(c)].

Calculated contour plots of the electron and heavy-hole wave functions reveal that for a wire height of 5 ML, the electron radius is much larger than that of the heavy hole in the direction of the wire height, and that the electron is indeed substantially spread out into the InP [Fig. 8 insets (a) and (b)]. This is made more quantitative in Fig. 8 by the calculation of the percentage of the electron and hole wave function inside the quantum wire as a function of the height of the quantum wire for a width of 180 Å. We now make a qualitative comparison of the numerical *electron* wave-

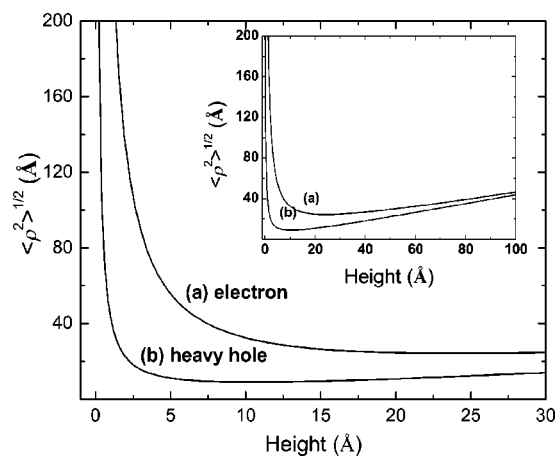


FIG. 9. Wave-function radii for (a) the electron and (b) the heavy hole in the [001] direction. The inset shows the same information but for much larger heights.

function radius with the experimental *exciton* extent. The theoretical data confirm the inverse dependence on the wire height up to 8 ML (24.24 Å) for the electron (Fig. 9). Between 4 and 5 ML the theoretical decrease in the electron wave-function radius with wire height is found to be 9%, which corresponds reasonably well with the experimental decrease in exciton wave-function extent of $\geq 5\%$ between HE and LE of sample C. For these flat wires, a considerable portion of the electron wave function is indeed found to be located above and below the quantum wire, i.e., 61% and 51% for heights of 4 and 5 ML, respectively (Fig. 8), resulting in respective electron wave-function radii of 2.9 and 2.6 nm in the [001] direction (Fig. 9).³⁰ The calculated electron wave-function radius for the 4 ML (12.12 Å) wire is thus almost five times larger than for a fully confined electron, for which the radius would be approximately half the wire height.

The wire height at which the exciton wave function is smallest indicates the regime in which the wave-function spillover starts to be significant, and is found to be at 8 ML (24.24 Å). This is only a factor of 2 smaller than the 50 Å that was experimentally and theoretically deduced for the $\text{In}_{0.1}\text{Ga}_{0.9}\text{As}/\text{GaAs}$ quantum well structures,^{9,15,17} although the confining potential for the electron is about five times larger in the InAs/InP wires.⁵

V. CONCLUSIONS

Magnetophotoluminescence experiments and theoretical calculations within the effective-mass approximation were combined to study the charge confinement in self-assembled InAs/InP quantum wire samples. Despite the large conduction band offset, the confinement energy for thin wires is large enough to cause a considerable portion of the electron wave function to be located outside the wire in the direction of the wire height. In this regime, a decrease of the electron wave-function extent is experimentally observed for increasing wire height in agreement with the theoretical calculations.

The wave-function penetration into the barrier is a crucial aspect that has to be kept in mind for applications since it reduces the electron-hole overlap and augments carrier escape at room temperature. To avoid these effects, growth procedures should be focused on enhancing the size uniformity of wires (and dots) with a height of at least 8 ML.

ACKNOWLEDGMENTS

This work is supported by the Belgian Science Policy and the Flemish Science Foundation (FWO-VI), the VIS projects of the KU Leuven and the UAntwerpen, the Nanoself project (TIC2002-04096-C03), and the NANOMAT project of the EC Growth program Contract No. G5RD-CT-2001-00545. B. P. is a post-doctoral researcher with the FWO-VI.

*Electronic mail: Jochen.maes@fys.kuleuven.ac.be

- ¹J. M. García, L. González, M. U. González, J. P. Silveira, Y. González, and F. Briones, *J. Cryst. Growth* **227**, 975 (2001).
- ²B. Alén, J. Martínez-Pastor, A. García-Cristobal, L. González, and J. M. García, *Appl. Phys. Lett.* **78**, 4025 (2001).
- ³L. González, J. M. García, R. García, F. Briones, J. Martínez-Pastor, and C. Ballesteros, *Appl. Phys. Lett.* **76**, 1104 (2000).
- ⁴M. U. González, J. M. García, L. González, J. P. Silveira, Y. González, J. D. Gómez, and F. Briones, *Appl. Surf. Sci.* **188**, 188 (2002).
- ⁵I. Vurgaftman, J. R. Meyer, and L. R. Ram-Mohan, *J. Appl. Phys.* **89**, 5815 (2001).
- ⁶J. Downes and D. Faux, *J. Appl. Phys.* **77**, 2444 (1995).
- ⁷C. Yi-Ping Chao and S. Chuang, *Phys. Rev. B* **46**, 4110 (1992).
- ⁸J. M. Worlock, F. M. Peeters, H. M. Cox, and P. C. Morais, *Phys. Rev. B* **44**, 8923 (1991).
- ⁹K. Oettinger, Al. L. Efros, B. K. Meyer, C. Woelk, and H. Brugger, *Phys. Rev. B* **52**, R5531 (1995).
- ¹⁰G. W. Bryant and Y. B. Band, *Phys. Rev. B* **63**, 115304 (2001).
- ¹¹R. Rinaldi *et al.*, *Phys. Rev. Lett.* **73**, 2899 (1994).
- ¹²G. Creci and G. Weber, *Semicond. Sci. Technol.* **14**, 690 (1999).
- ¹³H. Akiyama, *J. Phys.: Condens. Matter* **10**, 3095 (1998).
- ¹⁴L. Vescan, T. Stoica, and B. Holländer, *Mater. Sci. Eng., B* **89**, 49 (2002).
- ¹⁵S. N. Walck and T. L. Reinecke, *Phys. Rev. B* **57**, 9088 (1998).
- ¹⁶A. Balandin and S. Bandyopadhyay, *Phys. Rev. B* **52**, 8312 (1995).
- ¹⁷A. Thilagam, *Physica B* **262**, 390 (1999).
- ¹⁸H. M. Cox, D. E. Aspnes, S. J. Allen, P. Bastos, D. M. Hwang, S. Mahajan, M. A. Shahid, and P. C. Morais, *Appl. Phys. Lett.* **57**, 611 (1990).
- ¹⁹K. Kash, R. Bhat, D. D. Mahoney, P. S. D. Lin, A. Scherer, J. M. Worlock, B. P. Van der Gaag, M. Koza, and P. Grabbe, *Appl. Phys. Lett.* **55**, 681 (1989).
- ²⁰A. P. Roth, P. Finnie, S. Charbonneau, C. Lacelle, C. Guérini, J. Fraser, M. Buchanan, and Y. Feng, *Microelectron. J.* **28**, 909 (1997).
- ²¹S. Raymond, S. Studenikin, S.-J. Cheng, M. Pioro-Ladrière, M. Ciorga, P. J. Poole, and M. D. Robertson, *Semicond. Sci. Technol.* **18**, 385 (2003).
- ²²R. P. Schneider Jr. and B. W. Wessels, *J. Appl. Phys.* **70**, 405 (1991).
- ²³F. Guffarth, R. Heitz, A. Schliwa, K. Pötschke, and D. Bimberg, *Physica E (Amsterdam)* **21**, 326 (2004).
- ²⁴J. Maes, M. Hayne, M. Henini, F. Pulizzi, A. Patané, L. Eaves, and V. V. Moshchalkov, *Physica B* **346-347**, 428 (2004).
- ²⁵M. Hayne, R. Provoost, M. K. Zundel, Y. M. Manz, K. Eberl, and V. V. Moshchalkov, *Phys. Rev. B* **62**, 10324 (2000).
- ²⁶K. L. Janssens, F. M. Peeters, and V. A. Schweigert, *Phys. Rev. B* **63**, 205311 (2001).
- ²⁷E. Alphanbéry, R. J. Nicholas, N. J. Mason, S. G. Lyapin, and P. C. Klipstein, *Phys. Rev. B* **65**, 115322 (2002).
- ²⁸A. Shik, *Quantum Wells: Physics and Electronics of Two-dimensional Systems* (World Scientific, Singapore, 1997).
- ²⁹O. Stier, M. Grundmann, and D. Bimberg, *Phys. Rev. B* **59**, 5688 (1999).
- ³⁰Very recent calculations, which also include the effect of magnetic field are in good agreement with our magneto-optical data, and also yield exciton extents that are within 10% of those inferred from experiment.